Optimisation of accurate rutile TiO_2 (110), (100), (101) and (001) surface models from periodic DFT calculations

H. Perron, C. Domain, J. Roques, R. Drot, E. Simoni, H. Catalette

Title

Optimisation of Accurate Rutile TiO$_2$ (110), (100), (101) and (001) Surface Models from Periodic DFT Calculations

Authors

H. Perron[1, 2], C. Domain[1], J. Roques[2], R. Drot[2], E. Simoni[2], and H. Catalette[1]

Affiliation

[1] EDF–R&D, Département Matériaux et Mécanique des Composants, Les Renardières, Ecuelles, F–77818 Moret-sur-Loing Cedex, France.

[2] IPN Orsay UMR 8608, Université Paris XI, Bâtiment 100, F–91406 Orsay Cedex, France.

Corresponding author

J. Roques

e-mail: roques@ipno.in2p3.fr

Phone: +0033(1)69156869

Fax: +0033(1)69157150

Abstract

In this paper, geometric bulk parameters, bulk moduli, energy gaps and relative stabilities of the TiO$_2$ anatase and rutile phases were determined from periodic DFT calculations. Then, for the rutile phase, structures, relaxations and surface energies of the (110), (100), (101) and (001) faces were computed. The calculated surface energies are consistent with the natural rutile powder composition, even if a dependence on the number of layers of the slab used to model the surface was identified. Internal constraints, consisting in freezing some internal

layers of the slab to atomic bulk positions, were thus added to mimic the bulk hardness in order to stabilize the computed surface energies for thinner systems. In parallel, the influence of pseudopotentials was studied and it appears that four valence electrons for titanium atoms are sufficient. The aim of this study was to optimise accurate rutile TiO_2 surfaces models that will be used in further calculations to investigate water and uranyl ion sorption mechanisms.

Keywords

Rutile, TiO_2, DFT, surface.

1. Introduction

For years, the titanium dioxide, TiO_2, has been widely used as a white pigment and opacifier. Its recent application in catalysis and its photocatalysis properties make it a substrate of great interest from an experimental point of view as well as on a theoretical one. In the nature, this compound can be found under three crystallographic phases which are in order of decreasing abundance: rutile, anatase and brookite. A lot of microscopic studies carried out under ultra-high vacuum (UHV) conditions and with preliminary treatments (Ar^+-ion bombardment, irradiation, high temperature) have been performed especially considering some selected faces of the rutile phase, allowing a detailed knowledge at the atomic level in terms of relaxation and reconstruction [1-7]. Then, many metals and metal oxides overlayers growth [8-13], organic and inorganic molecules adsorption [14-21], have been also studied and the surface chemistry on this phase has been abundantly investigated. Among the low index faces naturally present in the rutile phase powder, the (110) face was found as the most stable one and thus has been much more studied than the others. In the case of the anatase phase, several

applications were found, for example in nanostructured solar cells. All these experimental investigations have besides been summarized by Diebold [22].

From a theoretical point of view, the rutile and anatase bulk phases and low index faces have been also investigated (see Diebold review article [22] and reference therein). Calculated intrinsic bulk parameters such as lattices parameters or bulk moduli were well reproduced [23]. The computed surface energies are also in agreement with the natural repartition of the different faces [24]. Adsorption studies also have been performed, especially on the rutile (110) face, with small organic molecules (H_2O, CO, NH_3, …) [25-29], atomic ions (Na^+, K^+, Ca^{2+}, …) [30-32] or metallic atoms (Au, Cu, Ag, …) [33-35], but some works have given opposite results. As an example, a disagreement arised for the adsorption of the water molecule on the rutile (110) face which is still a matter of controversy. Some authors found a spontaneous dissociation [36-37] while others agreed with a molecular adsorption mechanism [26,38]. This behaviour seems coming from the different models used (thickness and methods) showing the real importance of an accurate description of these surfaces. Experimental data suggests that the two forms may coexist simultaneously, and the relative proportions depend on several factors such as the initial oxygen vacancies density or pressure [39-41].

The regular increasing of the modern supercomputers power and the improvements of the methods allow to better describe the real systems. However, before studying solid/liquid interfacial reactions, a detailed knowledge of the surface, in terms of chemical and physical properties, should be beforehand established. Thus, it is of first importance to previously define well-characterised titanium dioxide TiO_2 surface models that could be then used as accurate models for studying complex adsorption processes. Among the previous *ab initio* calculations on TiO_2 rutile low index faces, several approaches have been used (Hartree-Fock or DFT in different formalisms) with multiple surface models. Nevertheless, to our

3

knowledge, no systematic comparison of the different surfaces as a function of the slab thickness with the same formalism has been performed.

In this paper, the (110), (100), (101) and (001) TiO_2 rutile surface properties have been characterised within the same DFT formalism based on the plane waves methodology. The ultrasoft pseudopotential (USPP) and projector augmented wave (PAW) formalisms are compared, as well as the effect of the number of valence electrons, on bulk properties and surface energies. A comparison of unconstrained and constrained surface models and the effect of the number of layers needed to reach convergence are also presented. Then, the surfaces relative stabilities and their atomic relaxations are correlated to their relative unsaturation and their structures. Finally, accurate (110), (100), (101) and (001) constrained surface models have been optimised to study sorption processes on large systems with a limited number of layers in order to speed up calculations.

2. Computational Details

All DFT periodic calculations were performed using the Vienna *ab initio* Simulation Package, VASP 4.6 [42-45], in local density approximation (LDA) and generalized gradient approximation (GGA as defined by Perdew and Wang [46]) formalisms, for the exchange-correlation energy evaluation. All atoms were described with pseudopotentials taken from the VASP library and developed on plane waves basis sets. Different pseudopotentials were used. The first ones are based on Vanderbilt-type [47-48] pseudopotentials also known as ultrasoft pseudopotentials (USPP). Titanium atoms were described by ten valence electrons ($3p^6 4s^2 3d^2$) and oxygen ones by six electrons ($2s^2 2p^4$). This first set of pseudopotentials will be referred as US10 in the following. The second set is generated with the Projector Augmented Wave

(PAW) method [49-50]. Two pseudopotentials were used for describing titanium atoms: the first one describes explicitly ten electrons ($3p^6 4s^2 3d^2$) and will be referred as PAW10; the second one, takes into account only four valence electrons ($3d^2 4s^2$), and will be noted PAW4. For oxygen atoms, a PAW pseudopotential with six valence electrons ($2s^2 2p^4$) was used. These two titanium PAW pseudopotentials were used in order to determine if the 3p electrons have to be included as semi-core in the pseudopotential to correctly describe the crystal properties. The Brillouin zone was integrated using the Monkhorst-Pack sets of k-points [51] (centered at the Γ point) depending on the supercell dimensions and of the number of atoms. Results for bulk relaxations were checked for convergence with respect to the number of k-points as well as energy cutoff. The density of states (DOS) calculations on the bulk were performed at the equilibrium volume using the tetrahedron method with Blöchl corrections for accuracy [52]. Except for calculating bulk parameters, all atomic relaxations were performed at constant volume (at the bulk equilibrium lattice parameters) by using the conjugate gradient optimisation scheme. All faces were built from direct bulk cleavage and thus exhibit undercoordinated atoms relative to their bulk structure. For each face, a sufficient vacuum thickness has been introduced between the slabs allowing to neglect their interaction.

3. Bulk Properties

This study started by optimising the rutile bulk parameters in order to build the faces and to determine the accuracy of the modelling by comparing calculated parameters to experimental ones. These first calculations were performed using different sets of k-points and energy cutoff to evaluate their effects on the bulk parameters and to optimise them. Relaxations were performed in two steps: the first one, with constant volume to optimise atom positions in the

lattice, and the second one, with unconstrained volume, to determine equilibrium bulk parameters and reference energies. In addition, the anatase phase lattice parameters were also determined in order to compare cohesive energies with the rutile phase.

The bulk rutile unit cell is tetragonal (a = b = 4.587 Å, c = 2.954 Å, internal parameter x = 0.305 and c/a = 0.644 [23]), space group No 136. Titanium atoms are in 2a positions and O atoms in 4f positions using Wyckoff's notations. The primitive cell contains two TiO_2 units.

For the LDA calculations, the optimised parameters (see Table 1) were obtained with an optimised 5×5×5 k-point mesh and a 400 eV cutoff, whereas for the GGA calculations the energy cutoff was optimised to 350 eV with the same k-point sampling. For a given functional (LDA or GGA), the results obtained with US10 and PAW10 pseudopotentials are similar. Moreover, only small differences can be noticed between PAW10 and PAW4 pseudopotentials showing that the four valence electrons are sufficient to correctly describe the titanium atoms and 3p semi-core electrons do not change significantly the results. Furthermore, this smaller number of electrons explicitly treated will allow to consider larger surfaces. By comparing to the experimental values, the LDA leads to a slight underestimation of the bulk parameters (around 0.04 and 0.03 Å on a and c parameters, respectively) while GGA gives an overestimation (0.04 and 0.02 Å on a and c parameters, respectively). Despite these little differences, there is a good agreement between calculated and experimental bulk parameters (1% error). Previous works from other groups gave similar results (see Table 1). Therefore, these different parameters have been used in all the coming constant volume relaxations.

The anatase phase is also tetragonal (a = b = 3.79 Å, c = 9.51 Å, internal parameter z = 0.208, c/a = 2.509 [23]), space group No 141. Titanium atoms are in 4a positions and oxygen ones in 8e. The elementary cell contains four TiO_2 units. Using the same sets of k-points and energy cutoff as for rutile, the anatase cell was optimised (see Table 2). Here, calculated values were

still in good agreement with experimental ones but it can be noticed that the c parameter is slightly overestimated in GGA that implies a largest error on the c/a ratio. This deviation has already been observed in the previous works reported in Table 2. Nevertheless, this error does not exceed 3% relatively to the experimental values.

The computed bulk moduli for anatase and rutile phases are also reported in Table 1 and 2. The bulk modulus measures the response in pressure, or resistance to a uniform compression, due to a change in the volume relative to the equilibrium one:

$$B = -V\frac{\partial P}{\partial V} = V\frac{\partial^2 E}{\partial V^2}, \qquad (1)$$

where E is the total energy of the supercell as a function of its volume V, P is the pressure and B the bulk modulus evaluated at the minimum of E.

In agreement with experimental results, the rutile's bulk modulus was always found higher than the anatase one whatever the functional (LDA or GGA) or the pseudopotential (US10, PAW10 or PAW4) used. For a given phase and functional, the US10 and PAW10 pseudopotentials gave similar results whereas the PAW4 one gave slightly higher values. The LDA calculations always lead to 30–40 GPa higher bulk moduli than GGA ones which were in better agreement with experimental values (rutile phase: 210 GPa [53-54], anatase phase: 180 GPa [55-56]).

The cohesive energy of the crystal can be calculated according to Eq. 2:

$$E_{coh} = \frac{E_{bulk} - N_{Ti}E_{Ti} - N_O E_O}{N_{TiO_2}}, \qquad (2)$$

where E_{Ti} is the reference energy for one titanium atom in the hexagonal compact crystal, E_O is the reference energy for oxygen atom in an isolated dioxygen molecule in gas phase, N_{Ti}, N_O and N_{TiO_2} are respectively the numbers of titanium atoms, oxygen atoms and TiO$_2$ units contained in the supercell and, finally, E_{bulk} is the total energy of the supercell. Using

==this definition, a negative value is favourable.== By comparing cohesive energies, the relative stability of these two phases can be calculated (see Table 3). The PAW4 pseudopotential gave about 10 meV energies lower than the two others pseudopotentials (PAW10 and US10). The relative energy stability is quite different when it is evaluated from LDA or GGA calculations. This disagreement has already been observed and these differences come from the exchange-correlation functionals used [57-58]. However, *ab initio* calculations always predict the rutile phase as the most stable one.

The energy gaps (difference between HOMO and LUMO) of the rutile and the anatase phases have been experimentally evaluated at 3.0 and 3.2 eV respectively [59]. The values calculated here, 1.6–1.9 eV and 1.9–2.3 eV for rutile and anatase respectively, are always lower (around 1–1.3 eV) relative to the experimental ones and depend strongly on the pseudopotential used. However, this result was predictable since it is known that DFT always underestimate gap energies because it is based on the description of the fundamental state and thus is not the most appropriate formalism to described excited states. Comparing the values obtained for the bulk with these three pseudopotentials, the set of pseudopotentials noted PAW4 (Ti: $4s^2 3d^2$, O: $2s^2 2p^4$) in this study gives accurate results.

4. Surfaces: Effect of the Slab Thickness

According to Jones et *al.* [60-61], it is known that rutile powder present three major crystallographic faces: (110), (101) and (100) with respectively a ratio of 60% / 20% / 20%. Surface energies were evaluated using Eq. 3:

$$E_{surf} = \frac{E_{slab} - E_{TiO_2} N_{TiO_2}}{2S},\qquad(3)$$

where E_{slab} is the total energy of the supercell, E_{TiO_2} the reference energy for a TiO_2 unit in bulk phase, N_{TiO_2} the number of TiO_2 unit in the supercell and S the surface area of one side of the slab depending on the considered face (see Table 4). For the four faces, a layer (L) has been defined as a plane containing titanium atoms. All atomic positions were able to relax during calculations.

4.1 Rutile (110) Face

The $TiO_2(110)$ face (Fig. 1-a) exhibits atoms with different environments. First, a pentacoordinated titanium atom, noted Ti(5), which is undercoordinated relative to its bulk structure. There are also two kinds of oxygen atoms, the first one is localised in the surface plane and is threefold coordinated (noted Os for "surface" oxygen); the second is prominent from the surface around 1 Å and is only doubly coordinated (noted Ob for "bridging" oxygen). All (110) surface energies were obtained using a 3×1×5 k-point grid (the system being $a\sqrt{2} \times (nL + vaccuum) \times c$). In Fig. 2, surface energies for systems from 1 to 13 layers are represented from LDA and GGA calculations with the three sets of pseudopotentials previously defined (US10, PAW10 and PAW4). It can be noted that the surface energy oscillates with the number of layers as already noted by Bates *et al.* [62] and Ramamoorthy *et al.* [24]. In a recent paper, Bredow *et al.* [63] have showed that the energy gap and the interlayer distances also oscillate with nL. However, the amplitude of these fluctuations decreases as the number of layers increases. Convergence was reached (within 0.02 J/m² for the three pseudopotentials) from the 10–12 layer systems. Referring to the converged surface energies, even nL gave smaller values and odd nL led to bigger ones. The differences between the LDA calculated surface energies and the GGA ones were important whatever the

pseudopotential used (about 0.4 J/m²) but, for a given formalism, they gave similar results. Atom displacements due to the surface relaxation were of various amplitude according to nL but remain in agreement with those experimentally observed [1-2] and calculated [24,26,62,64]. On the surface, the Ti–O bond lengths were modified relative to the bulk ones (two at 1.97 and one at 2.00 Å in GGA(PAW4)): d(Ti(6)–Ob) = 1.85 Å, d(Ti(6)–Os) = 2.05 Å. The Ti(5) atom falls down into the surface leading to a shortening of the remaining apical bond length at 1.83 Å. The calculated surface energies reported in the literature are always larger in GGA (0.73 [62], 0.81 [65] and 0.84 [66], in J/m²), while a better agreement was observed in LDA (0.89 [24], 0.84 [67] and 0.66 [68] in J/m²).

In agreement with the results on the bulk, the PAW4 pseudopotential gives similar results than the two other ones. Then, for the three following faces, (100), (101) and (001), the systematic study with the number of layers was performed only with the PAW4 pseudopotential.

4.2 Rutile (100) Face

The natural rutile powder is composed of about 20% of (100) face (Fig. 1-b). Although its "sawtooth" orientation, the (100) face exhibits exactly the same three kinds of atoms as the (110) face (see § IV.A). As for the (110) face, the surface energy was calculated with different number of layers (Fig. 3) with a 1×5×5 k-point mesh (with supercell dimensions: $(nL + vacuum) \times a \times c$). The (100) surface energy also oscillates with nL and the convergence was reached within 0.01 J/m² only from 8–10 layer systems (0.69 J/m² and 1.18 J/m² in GGA and LDA with PAW4 respectively) even if the amplitude of the oscillations is smaller than for the (110) face. These results are in agreement with values reported in the literature: 1.12 [24],

1.38 [69] and 1.30 [70] J/m² in LDA and 0.83 [69] J/m² in GGA. The (100) surface energy

was found to be higher than the (110) one which is in agreement with the fact that the (110)

face is the most stable one and with previous theoretical works [24,69]. The bond lengths on

the surface are also modified similarly to those observed on the (110) face. As previously

noted for the (110) face, the calculated LDA surface energies were always larger than the

GGA ones around 0.5 J/m² with the PAW4 pseudopotential. These calculations were also

performed with the PAW10 pseudopotential and gave similar results.

4.3 Rutile (101) Face

The (101) face (Fig. 1-c) is the third face occurring naturally in rutile powder for about 20%.

This face looks like the (100) one, it exhibits two kinds of atoms, first, a pentacoordinated

titanium, noted Ti(5); second, a twofold oxygen atom with two different Ti–O bond lengths,

noted O(2). The surface energy as a function of the number of layers was also calculated and

reveals a similar behaviour as for the other faces (Fig. 3), the k-point mesh used was 4×5×1

(with system dimensions: $\sqrt{a^2 + c^2} \times a \times (nL + vacuum)$). The converged surface energy (1.03

J/m² in GGA and 1.47 in LDA with PAW4) was reached, within 0.01 J/m², from 6-8 layer

systems. The (101) surface is also less table than the (110) one. These values are in agreement

with Ramamoorthy *et al.* [21] reporting 1.39 J/m² from LDA calculations and with the faces

repartition in natural rutile powder. Surface energies evaluated from LDA calculations are still

larger than the GGA ones around 0.4 J/m², as already noted for the (110) and the (100) faces.

The optimised Ti–O bond lengths on this surface are very different than those of the bulk (two

at 1.97 and one at 2.00 Å in GGA(PAW4)): 1.84 and 1.89 Å for the twofold oxygen atoms

while, for the threefold ones, 2.07 and 2.12 Å bond lengths were found. The PAW10 pseudopotential still gave similar results.

4.4 Rutile (001) Face

The dry (001) face (Fig. 1-d) does not belong to the three major faces present in powder however some experimental [22,70] and theoretical [24,71-74] works performed on this face are available in the literature. Then, this fourth face was investigated in order to make comparison with the three previous ones. This face also exhibits two kinds of atoms: a tetracoordinated titanium atom, noted Ti(4), with a high unsaturated valence and thus very acidic; and a twofold oxygen atom noted O(2). As above, the evolution of the surface energy with an increasing number of layers was studied (Fig. 3) with a 5×5×1 k-point mesh (the supercell being $a \times a \times (nL + vacuum)$). In this case, the space between two layers is very small (only $c/2 \approx 1.5$ Å) and, relative to the three other faces (around 3 Å), for an equivalent thickness, the number of layers is about twice than the three other ones. This explains why for the same number of layers, as for the three other faces, the surface energy is not converged and thus requires a higher number of layers. The fluctuations observed were as important as for the (110) one. Convergence within 0.1 J/m² was reached from 13–15 layer systems (1.25 J/m² and 1.76 J/m² in GGA and LDA with PAW4 respectively). The surface energy is larger than for the three previous faces in agreement with the fact that the (001) orientation has a minor contribution in the natural powder. This is also in agreement with the previous Ramamoorthy *et al.* [24] theoretical work giving in J/m²: 1.65 for the (001), 0.89 for the (110) and 1.12 for the (100). On this face, short Ti–O bond are also reported. The Ti(4) atom is surrounded by two oxygen atoms at 1.91 Å (O(2) on Fig. 1-d) and two others at 1.81 Å. As

12

for the three previous faces, the surface energies calculated from LDA calculations are larger than for the GGA ones around 0.5 J/m². Calculations with PAW10 are also in agreement with results obtained with PAW4.

As a last test, the influence of the three pseudopotentials on the computed GGA surface energies (from the biggest and fully relaxed systems) was studied, results are summarized in Table 5. For the four faces, the calculated surface energies, with the three pseudopotentials, were always in the same order: $E_{surf}^{US10} > E_{surf}^{PAW4} > E_{surf}^{PAW10}$, even if for the two PAW pseudopotentials, these values were nearly equal. An identical behaviour was observed with LDA calculations. Due to its "sawtooth" profile, the (100) face is composed of microfacets of $(a\sqrt{2})/2$ wide oriented in the [110] and the [$\bar{1}$10] directions. Therefore, the (100) face is thus, in a first approximation, equivalent to the (110) one with a $\sqrt{2}$ factor that is also found in the ratio of these two surface energies (see Table 5). Following these observations and those done previously for the bulk, it can be concluded that the PAW4 pseudopotential can correctly describe these systems. It has thus been used for all coming calculations.

5. Internal Constraints

5.1 Effects on the Surface Energies

Since the surface energies oscillate with nL, the models need to be described by slabs composed of a large number of layers to reach convergence. However, to study large surfaces, the number of layers needs to be the smallest as possible. In this way, internal constraints were added in the slabs. The surface energies and the atomic relaxations have been used to find the best compromise between size and accuracy. These constraints consist in freezing some of the most internal layers to their bulk atomic positions. They introduce the hardness of

13

the bulk that isolates the relaxation of each side of the slab from one to the others and thus decrease size effects. There are several possibilities to add these constraints. As an example, for a five layers system, if only the most internal layer is frozen, the two external layers on each side of the slab will be able to relax, while if the three most internal layers are frozen, only the most external layer on each side will be able to relax. These systems are noted nL_m with n the number of layers and m the number of layers able to relax on each side. The surface energies of the totally constrained systems (noted Unrelaxed) were also calculated for comparison. Similar studies on partially constrained systems have already been performed by Thompson *et al.* [75] and Hameeuw *et al.* [76], on the (110) face only and focus more particularly on geometrical parameters. All the following calculations were performed in GGA with the PAW4 pseudopotential.

Surface energies of the constrained (110) face are reported in Fig. 4-a. For the most constrained systems (Unrelaxed), the surface energies are larger around 0.8–0.9 J/m² relative to the totally unconstrained ones (Fully relaxed), but the parity of nL has smaller effects. By unconstraining slightly these systems (nL_1), the surface energies decrease significantly around 0.6–0.7 J/m² and the oscillation with nL parity becomes smaller. By again unconstraining these systems (nL_2), the surface energies still decrease (around 0.1 J/m²) and stay quasi-stable with nL. For the last systems (nL_3), there is no significant difference relative to the nL_2 ones. For the three nL_m systems, surface energy convergence is here reached within 0.02 J/m² for 5–8 layer systems, even if these converged energies are larger than the one of the totally unconstrained systems.

For the (100) face (see Fig. 4-b), the energies of the unrelaxed systems are larger by more than 0.8 J/m² as for the (110) face. The progressive relaxation of the external layers has significant effects on the surface energies and, the 3L_1 case excepted, the surface energies are linear with nL for the 3 constrained systems. Since the surface energy of the 5L_2 system

(0.71 J/m²) is close the converged one (0.69 J/m²), this constrained system is a good compromise to model the (100) surface.

The internal constraints were then added to the (101) face slabs (see Fig. 4-c). The effects were the same as for the two previous faces. The energy of the unrelaxed surface is larger by 0.6 J/m² relative to the converged one. For a 5L_2 system, the calculated surface energy is 1.05 J/m² which is very close to the converged one for the fully relaxed system with 1.03 J/m². As observed for the (100) face, only the surface energies of the fully relaxed systems oscillate while those of the constrained ones are linear with the number of layers.

Finally, these internal constraints were added to the (001) face (see Fig. 4-d). The effects on the surface energies were exactly the same as for the (110) face: i) high surface energies for the unrelaxed systems (about 2.3 J/m²); ii) accurate stability with nL but larger surface energy for the second most constrained systems (nL_2); iii) net decrease of the surface energy for the nL_4 and nL_6 systems; iv) the surface energy is then very close to that of the fully relaxed systems. By adding the constraints, the convergence was reached with 8–10 layer systems.

Four surface models have been optimised: five layer slabs with their most internal layer frozen to bulk positions for the (110), (100) and (101) face and a nine layer slab with the same constraint for the (001) face. These constrained models have been used in the following calculations.

5.2 Surface Unsaturation and Relative Energies

The relative stabilities of these four surfaces can be explained by their respective unsaturation. In Table 6 are reported the unsaturated valence densities, from GGA(PAW4) calculations, for titanium and oxygen atoms per nm², defined as the number of "broken bonds", relative to

their bulk coordination (6 for titanium atoms and 3 for oxygen ones). The (110) face has the lowest number of unsaturated valence per nm² and is also the most stable face, followed by the (100) and then the (101) ones. The (001) face is the less stable one with a higher surface energy relative to the (110) one. The relaxed surface energies were found to increase with the surface densities of unsaturated sites (considering Ti and O simultaneously). The relaxed surface energy is thus directly linked to its unsaturation. The more the surface is unsaturated, the less it is stable. This correlation was also observed for the converged surface energies whatever the functional or the pseudopotential used (see Table 5).

In Table 6, the relaxed surface bond lengths are also reported and compared to the calculated bulk ones. These deviations were correlated to the unsaturation of the surface because the more it is unsaturated, the more the bond lengths should be modified. The smallest deviations were observed for the (110) and the (100) faces. For the threefold oxygen atoms, these deviations were more important for the (101) and then for the (001) faces. Regarding the twofold oxygen atoms, only bond shortening were observed with similar amplitude for the four faces. Considering the threefold oxygen atoms, a bond lengthening was observed in the case of the (110), (100) and (101) faces while a shortening occurred for the (001) face. This behaviour can be explained by the fact that the titanium atoms are fivefold coordinated for the (110), (100) and (101) faces while they are only fourfold coordinated on the (001) face.

6. Conclusion

First-principles calculations on the titanium dioxide crystals and on the TiO_2 rutile surfaces were performed in order to build accurate surface models which could be used to investigate surface defects, reconstruction or adsorption processes.

First, the lattice bulk parameters, the bulk moduli, the gap energies and the relative energies of rutile and anatase phases were calculated. The computed lattice bulk parameters and bulk moduli were found to be in good agreement with experimental data and previous theoretical works. The rutile phase was always found as the most stable one. It was found that the calculated energy gaps underestimate the experimental values as already mentioned for other systems from DFT calculations. Nevertheless, it appears that four valence electrons for titanium atoms and six for oxygen ones with the PAW pseudopotential formalism are well adapted to correctly describe bulk properties.

Secondly, rutile low index faces were investigated. In agreement with the natural rutile powder composition, the (110) face was found as the most stable one, followed by the (100) and the (101) ones. The (001) face was also studied and its calculated surface energy is much higher than the three previous faces. A nearly linear correlation between the four surface energies and their respective unsaturation and relaxation amplitude was highlighted. In addition, it was observed that the surface energies of these four faces depend on the number of layers used in the slab to model the system. Internal constraints were thus added in the slabs for the four faces to stabilise their surface energies. These constrained systems allowed to build stable surface models for smaller slab thicknesses than the unconstrained ones. For the (110), (100) and the (101) faces, five layer models with their most internal layer frozen to bulk positions were found to be a good compromise to model these faces. Finally, for the (001) face, a nine layer slab with its most internal layer frozen to bulk positions was determined as an accurate model. Comparing the effect of the pseudopotentials (US10, PAW10 and PAW4), it was found that the one noted PAW4 in this study can be used to properly describe these systems.

Consequently, these four constrained surface models with PAW pseudopotentials (Ti: $3s^2 4p^2$ and O:$2s^2 2p^4$) could be used to investigate, with a good accuracy, adsorbates–(TiO$_2$ surface)

interactions or surface reconstruction phenomenon. The (110) face constrained model have been used to study the co-adsorption of molecular and dissociated water molecules [77] and to investigate the uranyl ion sorption [78] that are compared to experimental data [16,79].

Acknowledgments

References

1. Lindsay R, Wander A, Ernst A, Montanari B, Thornton G, Harrison NM (2005) Phys Rev Lett 94:246102

2. Charlton G, Howes PB, Nicklin CL, Steadman P, Taylor JSG, Muryn CA, Harte SP, Mercer J, McGrath R, Norman D, Turner TS, Thornton G (1997) Phys Rev Lett 78:495

3. Czyzewski JJ, Krajniak J, Klein S (2004) App Surf Sci 227:144

4. Diebold U, Lehman J, Mahmoud T, Kuhn M, Leonardelli G, Hebenstreit W, Schmidt M, Varga P (1998) Surf Sci 411:137

5. Fischer S, Munz AW, Schierbaum KD, Göpel W (1995) Surf Sci 337:17

6. Murray PW, Condon NG, Thornton G (1995) Phys Rev B 51:10989

7. Novak D, Garfunkel E, Gustafsson T (1994) Phys Rev B 50:5000

8. Zhang Z, Fenter P, Cheng L, Sturchio NC, Bedzyk MJ, Machesky ML, Anovitz LM, Wesolowski DJ (2006) J Coll Int Sci 295:50

9. Agnoli S, Sambi M, Granozzi G, Castellarin-Cudia C, Surnev S, Ramsey MG, Netzer FP (2004) Surf Sci 562:150

10. Tanner RE, Goldfarb I, Castell MR, Briggs GAD (2001) Surf Sci 486:167

11. Towle SN, Brown Jr GE, Parks GA (1999) J Coll Int Sci 217:299

12. Ridley MK, Machesky ML, Wesolowski DJ, Palmer DA (1999) Geochim Cosmochim Acta 63:3087

13. O'Day PA, Chisholm-Brause CJ, Towle SN, Parks GA, Brown Jr GE (1996) Geochim Cosmochim Acta 60:2515

14. Onda K, Li B, Zhao J, Petek H Surf Sci (2005) 593:32

15. Olsson M, Jakobsson AM, Albinsson Y (2003) J Coll Int Sci 266:269

16. Den Auwer C, Drot R, Simoni E, Conradson SD, Gailhanou M, Mustre de Leon J (2003) New J Chem 27:648

17. Rodriguez JA, Hrbek J, Chang Z, Dvorak J, Jirsak T (2002) Phys Rev B 65:235414

18. Robert D, Parra S, Pulgarin C, Krzton A, Weber JV (2000) Appl Surf Sci 167:51

19. Henderson MA (1998) Surf Sci 400:203

20. Shultz AN, Hetherington III WM, Baer DR, Wang LQ, Engelhard MH (1997) Surf Sci 392:1

21. Hadjiivanov K (1988) Appl Surf Sci 135:331

22. Diebold U (2003) Surf Sci Rep 48:53

23. Muscat J, Swamy V, Harrison NM (2002) Phys Rev B 65:224112

24. Ramamoorthy M, Vanderbilt D, King-Smith RD (1994) Phys Rev B 49:16721

25. Jug K, Nair NN, Bredow T (2005) Surf Sci 590:9

26. Bandura AV, Sykes DG, Shapovalov V, Troung TN, Kubicki JD, Evarestov RA (2004) J Phys Chem B 108:7844

27. Zhang C, Lindan PJD (2003) Chem Phys Lett 373:15

28. Langel W, Menken L (2003) Surf Sci 538:1

29. Odelius M, Persson P, Lunell S (2003) Surf Sci 529:47

30. Předota M, Zhang Z, Fenter P, Wesolowski DJ, Cummings PT (2004) J Phys Chem B 108:12061

31. Svetina M, Colombi Ciacchi L, Sbaizero O, Meriani S, De Vita A (2001) Acta Mater 49:2169

32. Muscat J, Harrison NM, Thornton G (1999) Phys Rev B 59:15457

33. Wang Y, Hwang GS (2003) Surf Sci 542:72

34. Lopez N, Nørskov JK (2002) Surf Sci 515:175

35. Giordano L, Pacchioni G, Bredow T, Sanz JF (2001) Surf Sci 471:21

36. Menetrey M, Markovits A, Minot C (2003) Surf Sci 524:49

37. Ahdjoudj J, Markovits A, Minot C (1999) Catal Today 50:541

38. Barnard AS, Zapol P, Curtiss LA (2005) J Chem Theory Comput 1:107

39. Wang LQ, Baer DR, Engelhard MH, Shultz AN (1995) Surf Sci 344:237

40. Brookes IM, Muryn CA, Thornton G (2001) Phys Rev Lett 87:266103

41. Schaub R, Thostrup P, Lopez N, Lægsgaard E, Stensgaard I, Nørskov JK, Besenbacher JF (2001) Phys Rev Lett 87:266104

42. Kresse G, Hafner J (1993) Phys Rev B 47:R558

43. Kresse G, Hafner J (1994) Phys Rev B 49:14251

44. Kresse G, Furthmüller J (1996) Comput Mater Sci 6:15

45. Kresse G, Furthmüller J (1996) Phys Rev B 54:11169

46. Perdew JP, Wang Y (1992) Phys Rev B 45:13244

47. Vanderbilt D (1985) Phys Rev B 32:8412

48. Vanderbilt D (1990) Phys Rev B 41:R7892

49. Blöch PE (1994) Phys Rev B 50:17953

50. Kresse G, Joubert D (1999) Phys Rev B 59:1758

51. Monkhorst HJ, Pack JD (1976) Phys Rev B 13:5188

52. Blöchl PE, Jepsen O, Andersen OK (1994) Phys Rev B 49:16223

53. Gerward L, Olsen JS (1997) J Appl Crystallogr 30:259

54. Ming LC, Manghani MH (1979) J Geophys Res 84:4777

55. Arlt T, Bermejo M, Blanco MA, Gerward L, Jiang JZ, Olsen JS, Recio JM (2000) Phys Rev B 61:14414

56. Swamy V, Gale JD, Dubrovinsky LS (2001) J Phys Chem Solids 62:887

57. Fahmi A, Minot C, Silvi B, Causá M (1993) Phys Rev B 47:11717

58. Causá M, Zupan A (1994) Chem Phys Lett 220:145

59. Kavan L, Grätzel M, Gilbert SE, Klemenz C, Scheel HJ (1996) J Am Chem Soc 118:6716

60. Jones P, Hockey JA (1971) Trans Faraday Soc 67:2669

61. Jones P, Hockey JA (1971) Trans Faraday Soc 67:2679

62. Bates SP, Kresse G, Gillan MJ (1997) Surf Sci 385:386

63. Bredow T, Giordano L, Cinquini F, Pacchioni G (2004) Phys Rev B 70:035419

64. Bandura AV, Kubicki JD (2003) J Phys Chem B 107:11072

65. Lindan PJD, Harrison NM, Gillan MJ, White JA (1997) Phys Rev B 55:15919

66. Goniakowski J, Gillan MJ (1996) Surf Sci 350:145

67. Lazzeri M, Vittadini A, Selloni A (2001) Phys Rev B 63:155409

68. Albaret T, Finocchi F, Noguera C, De Vita A (2001) Phys Rev B 65:035402

69. Lindan PJD, Harrison NM, Holender JM, Gillan MJ, Payne MC (1996) Surf Sci 364:431

70. Muscat J, Harrison NM, Thornton G (1999) Phys Rev B 59:2320

71. Tero R, Fukui KI, Iwasawa Y (2003) J Phys Chem B 107:3207

72. Munnix S, Schmeits M (1984) Phys Rev B 30:2202

73. Mackrodt WC, Simson EA, Harrison NM (1997) Surf Sci 384:192

74. Muscat J, Harrison NM (2000) Surf Sci 446:119

75. Thompson SJ, Lewis SP (2006) Phys Rev B 73:073403

76. Hameeuw KJ, Cantele G, Ninno D, Trani F, Iadonisi G (2006) J Chem Phys 124:024708

77. Perron H, Vandenborre J, Domain C, Roques J, Drot R, Simoni E, Catalette H, Surface Science, accepted

78. Perron H, Domain C, Roques J, Drot R, Simoni E, Catalette H (2006) Inorg Chem Com 45:6568

79. Dossot M, Cremel S, Vandenborre J, Grausem J, Humbert B, Drot R, Simoni E (2006) Langmuir 22:140

Table 1. Optimised rutile bulk parameters (in Å), bulk moduli (in GPa) and energy gaps (in eV). Data from previous studies: GGA and LDA using plane waves, and HF using linear combination of atomic orbitals, are also reported.

	a	c	x	c/a	B	Gap
Exp.	4.587	2.954	0.305	0.644	210	3.0[b]
GGA(US10)	4.639	2.983	0.305	0.643	218	1.90
GGA(PAW10)	4.642	2.973	0.305	0.640	217	1.80
GGA(PAW4)	4.649	2.972	0.304	0.640	225	1.65
LDA(US10)	4.554	2.937	0.304	0.645	254	1.94
LDA(PAW10)	4.554	2.927	0.304	0.643	256	1.81
LDA(PAW4)	4.561	2.929	0.303	0.642	263	1.66
GGA[a]	4.651	2.964	0.307	0.637	—	—
LDA[a]	4.574	2.927	0.304	0.640	—	—
HF[a]	4.575	2.999	0.306	0.656	239	—

[a] [23]. [b] [59].

Table 2. Optimised anatase bulk parameters (in Å), bulk moduli (in GPa) and energy gaps (in eV). Data from previous studies: GGA and LDA using plane waves, and HF using linear combination of atomic orbitals, are also reported.

	a	c	z	c/a	B	Gap
Exp.	3.782	9.502	0.208	2.512	180	3.2[b]
GGA(US10)	3.794	9.822	0.205	2.589	191	2.30
GGA(PAW10)	3.804	9.724	0.206	2.557	189	2.08
GGA(PAW4)	3.810	9.726	0.206	2.552	199	1.93
LDA(US10)	3.751	9.498	0.208	2.532	219	2.22
LDA(PAW10)	3.747	9.488	0.208	2.532	219	2.04
LDA(PAW4)	3.756	9.497	0.208	2.528	226	1.94
GGA[a]	3.792	9.714	0.206	2.562	—	—
LDA[a]	3.758	9.495	0.208	2.527	—	—
HF[a]	3.781	9.735	0.203	2.575	202	—

[a] [23]. [b] [59].

Table 3. Relative stabilities between rutile and anatase phases (in meV).

Refs	$E_{coh}(rutile) - E_{coh}(anatase)$
GGA(US10)	–86
GGA(PAW10)	–83
GGA(PAW4)	–75
LDA(US10)	–24
LDA(PAW10)	–24
LDA(PAW4)	–11
GGA[a]	–74
LDA[a]	–34
LDA[b]	–20

[a] [23]. [b] [66].

Table 4. Rutile face's unit surface area and the corresponding k-point grid.

	Unit surface area (Å²)	k-point grid[a]	Space between layers
(110)	$a\sqrt{2} \times c$	3×1×5	$(a\sqrt{2})/2$
(100)	$a \times c$	1×5×5	$a/2$
(101)	$a \times \sqrt{a^2 + c^2}$	4×5×1	c
(001)	$a \times a$	5×5×1	$c/2$

[a]The surface normal is along the axe with one k-point.

Table 5. Converged surface energies (in J/m²) calculated from the biggest systems in GGA for the three pseudopotentials.

Face	E_{surf}^{US10}	E_{surf}^{PAW4}	E_{surf}^{PAW10}
(110)	0.54	0.50	0.48
(100)	0.76	0.69	0.67
(101)	1.08	1.03	1.01
(001)	1.32	1.25	1.21

Table 6. Surface energies for the four constrained surface models (in J/m²) and their unsaturation (per nm²) from GGA(PAW4) calculations. Effects on the relaxed Ti–O surface bond lengths (in Å) relative to the bulk ones (1.97 and 2.00 Å, deviation in parenthesis in Å).

	$E_{constrained}^{PAW4}$	Unsaturation	Twofold oxygen atoms	Threefold oxygen atoms
(110)	0.60	10.23	1.85 (-0.12)	2.06 (+0.06)
(100)	0.71	14.47	1.86 (-0.11)	2.06 (+0.06)
(101)	1.05	15.59	1.83 (-0.14)	2.05 (+0.08)
			1.90 (-0.10)	2.12 (+0.12)
(001)	1.38	18.50[a]	1.88 (-0.09)	1.82 (-0.15)
			1.90 (-0.10)	

[a] There is only one unsaturated Ti per (001) unit area but it has 2 unsaturated valences instead of only one for the three other faces.

Figure Captions:

Figure 1. The dry rutile (a) (110), (b) (100), (c) (101) and (d) (001) faces.

Figure 2. Rutile (110) surface energy as a function of the slab thickness for 1 to 13 layer systems (in J/m²). nL is the number of layers.

Figure 3. Rutile (100), (101) and (001) surface energy as a function of the slab thickness with the PAW4 pseudopotential (in J/m²) from GGA and LDA calculations.

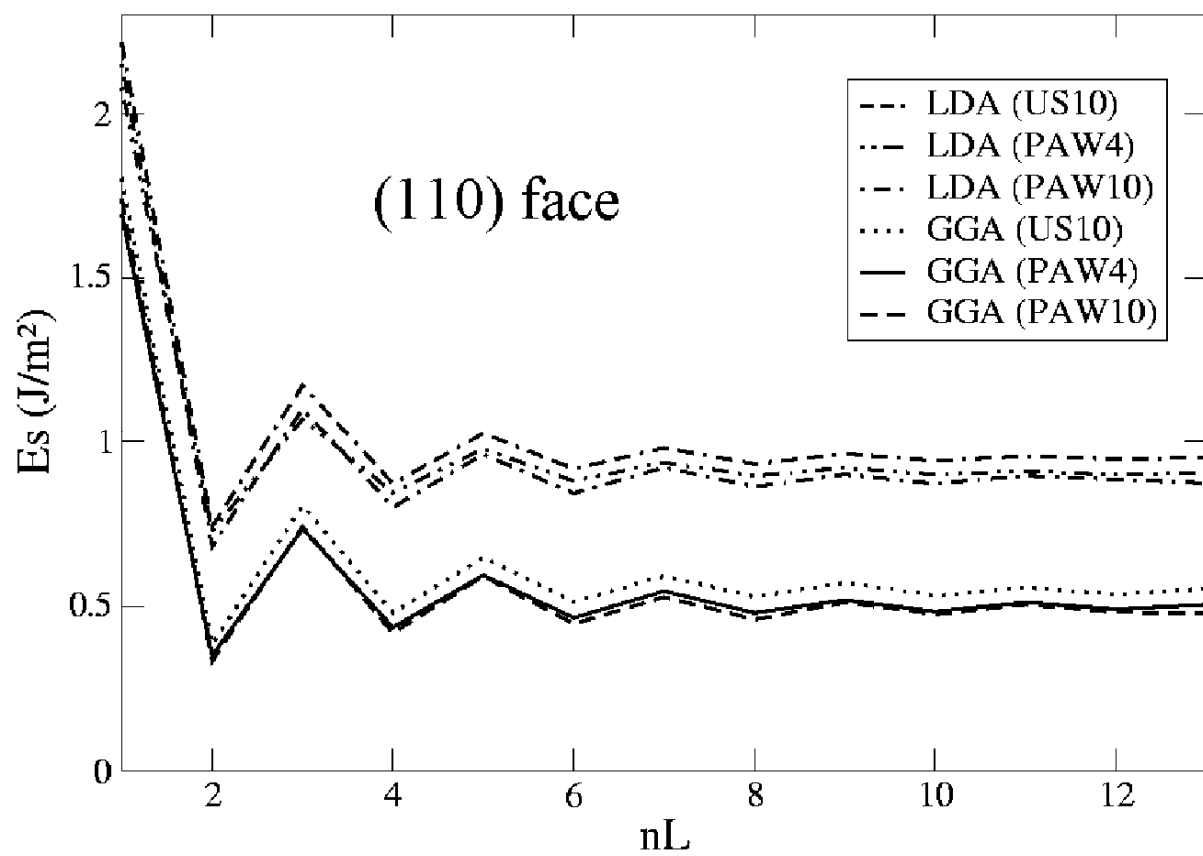Figure 4. Effect of internal constraints on surface energies (in J/m²) from GGA(PAW4) calculations: (a) (110), (b) (100), (c) (101) and (d) (001).
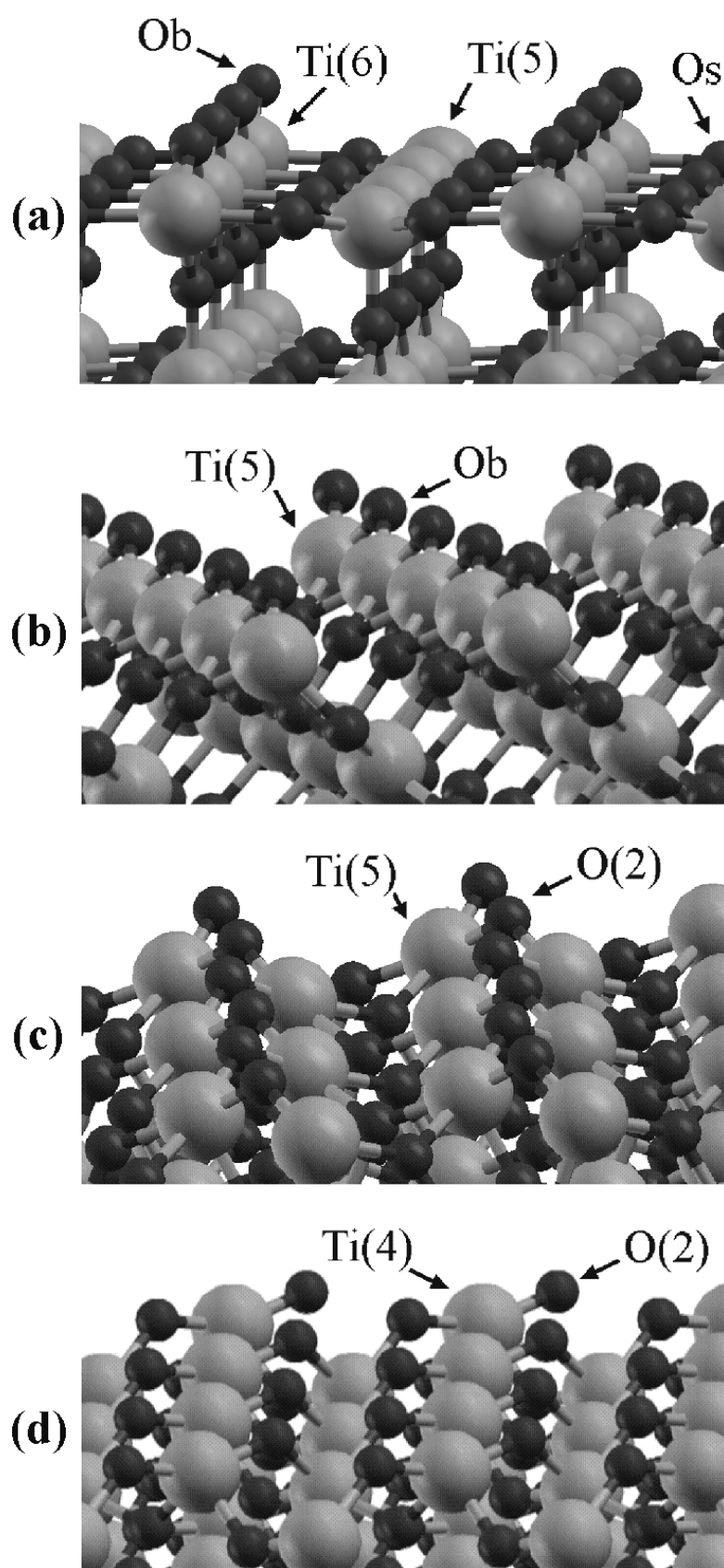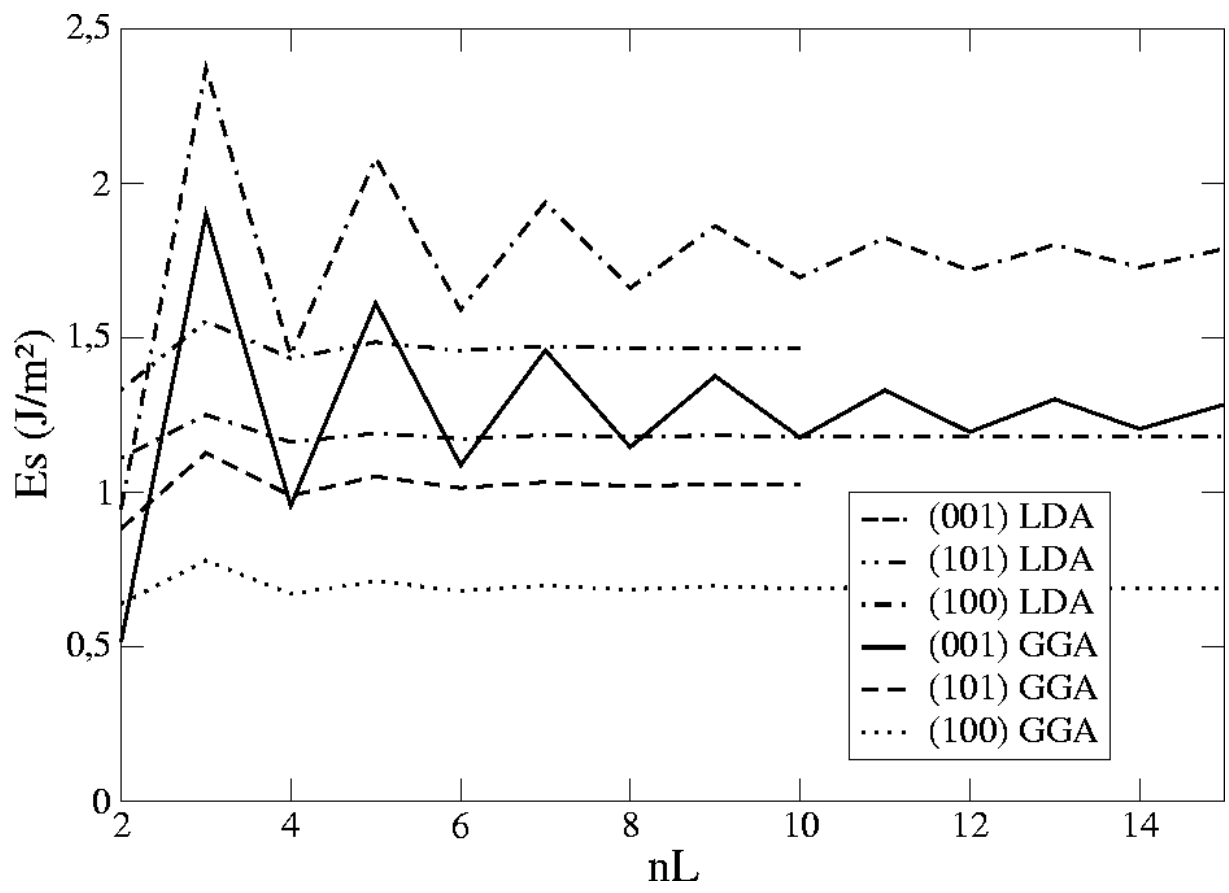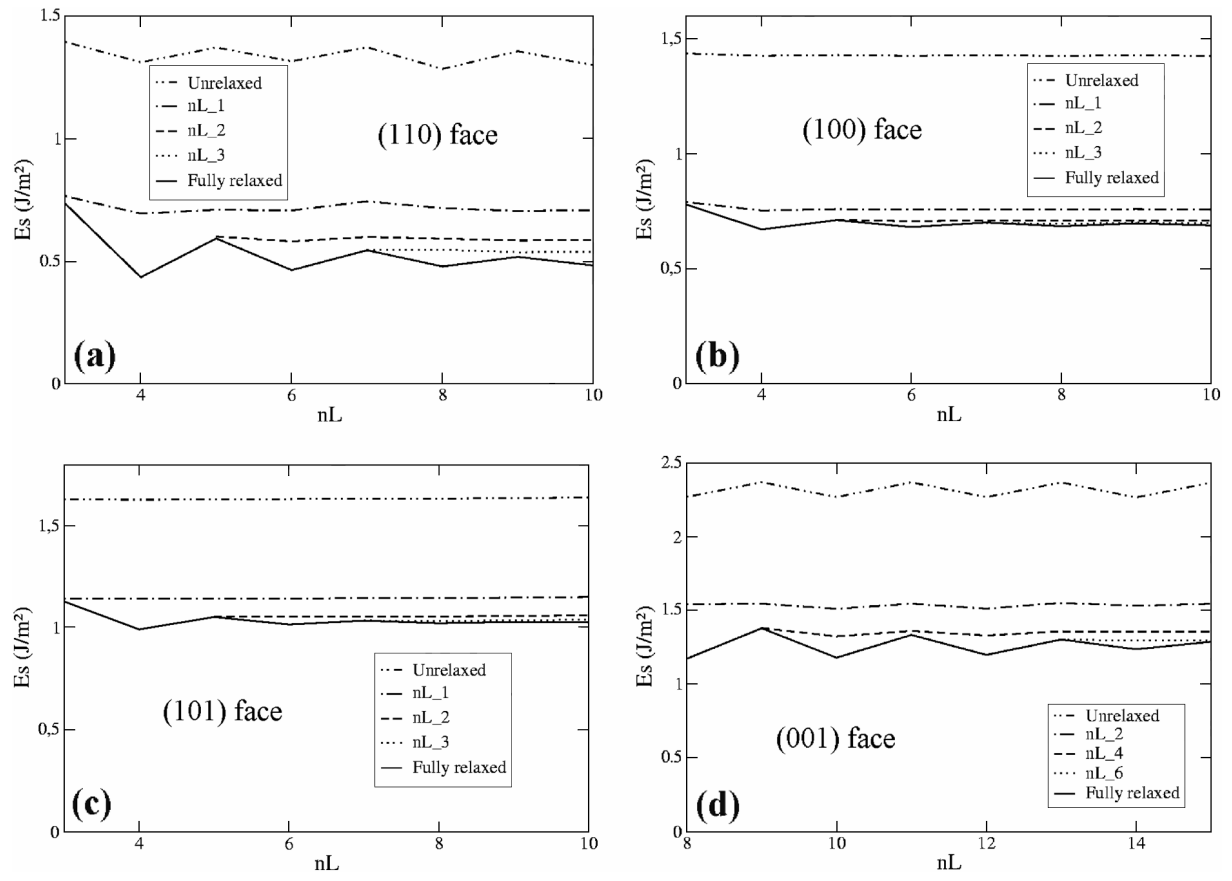
Figure 1.

Figure 2.

Figure 3.

Figure 4.